

# 3D spectroscopy of merger Seyfert galaxy Mrk 334: nuclear starburst, superwind and the circumnuclear cavern

Aleksandrina Smirnova<sup>1\*</sup> and Alexei Moiseev<sup>1</sup>

<sup>1</sup>*Special Astrophysical Observatory, Russian Academy of Sciences, Nizhnii Arkhyz, Karachaevo-Cherkesskaya Republic, 369167 Russia*

11 September 2021

## ABSTRACT

We are presenting new results on kinematics and structure of the Mrk 334 Seyfert galaxy. Panoramic (3D) spectroscopy is performed at the 6-m telescope of the Special Astrophysical Observatory of the Russian Academy of Sciences using the MPFS integral-field spectrograph and scanning Fabry–Pérot interferometer. The deep images have revealed that Mrk 334 is observed during the final stage of its merging with a massive companion. A possible mass ratio ranges from 1/5 to 1/3. The merger has triggered mass redistribution in the disk resulting in an intensification of nuclear activity and in a burst of star formation in the inner region of the galaxy. The circumnuclear starburst is so intense that its contribution to the gas ionization exceeds that contribution of the AGN. We interpret the nuclear gas outflow with velocities of  $\sim 200 \text{ km s}^{-1}$  as a galactic superwind that accompanies the violent star formation. This suggestion is consistent with the asymmetric X-ray brightness distribution in Mrk 334. The trajectory of the fragments of the disrupted satellite in the vicinity of the main galaxy nucleus can be traced. In the galaxy disk a cavern is found that is filled with a low-density ionized gas. We consider this region to be the place where the remnants of the companion have recently penetrated through the gaseous disk of the main galaxy.

**Key words:** galaxies: Seyfert – galaxies: individual: Mrk 334 – galaxies: kinematics and dynamics – galaxies: interactions – galaxies: starburst

## 1 INTRODUCTION

Numerical simulations demonstrate that galaxy interaction stimulates a concentration of gas in its central regions, thereby triggering nuclear activity and/or a burst of star formation (Barnes & Hernquist 1991; Springel, Di Matteo & Hernquist 2005; Bekki, Shioya & Whiting 2006). Many authors have tried to find a correlation between an AGN phenomenon and galaxy environment: the presence of companions or traces of interaction (Dahari 1985; De Robertis, Yee & Hayhoe 1998; Schmitt 2001; Knapen 2005). However, statistically significant correlation has not been found.

A number of authors suggest that the activity may be triggered and sustained by a complex mechanism that includes several factors (see Martini (2004) and the references therein). It is clear that only a detailed analysis of the kinematics and dynamics of both the inner (100 – 1000 pc scale) and outer regions in active galaxies would make it possible to understand how in each particular case the ‘fuel’ (interstellar

gas) is brought into the domain of action of the gravitational forces of the AGN ‘central engine’.

This paper continues a series of papers dedicated to a detailed study of the inner kinematics of active galaxies via methods of panoramic (3D) spectroscopy. This technique provides spectra for every spatial element (‘spaxel’) of a two-dimensional field of view. It is a powerful tool for studying non-circular motions and gas ionization properties both in the circumnuclear and external regions. Our work is aimed to investigate the relation between the gas kinematics, morphological features and nuclear activity in individual galaxies as well as the mechanisms of the central region feeding. We have already published the results concerning Mrk 315 (Ciroi et al. 2005), NGC 6104 (Smirnova, Moiseev & Afanasiev 2006), and Mrk 533 (Smirnova et al. 2007). In this paper we report a detailed study of Mrk 334.

Mrk 334 (VV 806, UGC 6) is a peculiar galaxy with Sy1.8 nucleus (according to the NED database). This object has been popular among the researchers due to its peculiar appearance on optical images: it has an asymmetric eastward-extending arm (Vorontsov-Vel’yaminov

\* ssmirnova@gmail.com

1977) and a bright H $\alpha$  condensation near the nucleus (Gonzalez Delgado et al. 1997). The latter authors suggested that the object actually consisted of two merging galaxies. Mrk 334 is notable for violent star formation, resulting in high IR luminosity  $L_{IR} = 8.9 \times 10^{11} L_{\odot}$  (Pérez García & Rodríguez Espinosa 2001). Rothberg & Joseph (2004) classify it as a luminous infrared galaxy (LIRG). Maiolino et al. (1997) suggested that the peculiarities in the structure of the galaxy are indicative of its recent interaction with a companion, which has triggered the nuclear activity. However, when and what did the galaxy interact with? In the present paper we try to answer this question and to look for the feedback effects between the central and surrounding regions.

The paper has the following layout. Section 2 describes the observations and the data reduction; Section 3 analyses the distribution of ionized gas and stars both in the inner disk and in the outer regions of the galaxy. Section 4 analyses the ionization state of selected regions in Mrk 334, and in Section 5 the kinematics of the gas and stars are considered. Section 6 studies the peculiarities of X-ray radiation according to the *ROSAT* data, and Section 7 includes an overall discussion of the whole galaxy structure and the circumnuclear ionized gas cavern.

The adopted distance to the galaxy — 91.4 Mpc (Maiolino et al. 1997) corresponds to a scale of 443 pc/arcsec (for redshift  $z=0.022$  and  $H_0 = 75 \text{ km s}^{-1} \text{ Mpc}^{-1}$ ).

## 2 OBSERVATIONS AND DATA REDUCTION

All observations were made in the prime focus of the 6-m telescope of the Special Astrophysical Observatory of the Russian Academy of Sciences (SAO RAS). Table 1 provides the log of the observations. The central region of Mrk 334 was observed with the Multi-Pupil Fiber Spectrograph (MPFS). The large-scale kinematics and galactic environment were studied using the SCORPIO multi-mode focal reducer operating in the modes of scanning Fabry–Pérot interferometer (FPI) and broad-band imaging. The detectors used in 2006 and 2002 were a CCD EEV42-40 ( $2048 \times 2048$  pixels) and a CCD TK1024 ( $1024 \times 1024$  pixels), correspondingly.

### 2.1 MPFS integral-field spectrograph

The integral-field spectrograph MPFS (Afanasiev et al. 2001) takes simultaneous spectra of 256 spatial elements arranged in the form of  $16 \times 16$  square lenses array with a scale of 1 arcsec per spaxel. Behind each lens an optical fibre is located whose other end is packed into the spectrograph slit. The sky background spectrum was simultaneously taken with 17 additional fibres located 4 arcmin away from the object. The wavelength interval included numerous emission lines of ionized gas and absorption features of the stellar population.

The preliminary data reduction steps were described earlier (Moiseev et al. 2004; Smirnova et al. 2007). Reduction yields a ‘data cube’, where each pixel in the  $16 \times 16$  arcsec field has a spectrum associated with it. The spectra of the spectrophotometric standard stars were used

**Table 1.** Log of the observations.

Date	Instrument	Exp. time, s	Sp. range	Sp. resol.	seeing arcsec
23.11.2006	MPFS	7200	3740 – 5850 Å	6.5 Å	1.4
		7200	4300 – 7220 Å	6.5 Å	1.4
05.09.2002	SCORPIO (FPI)	6400	H $\alpha$	2.8 Å	1.3
23.10.2006	SCORPIO (Images)	660	<i>V</i>		1.4
		1020	<i>R</i>		1.4

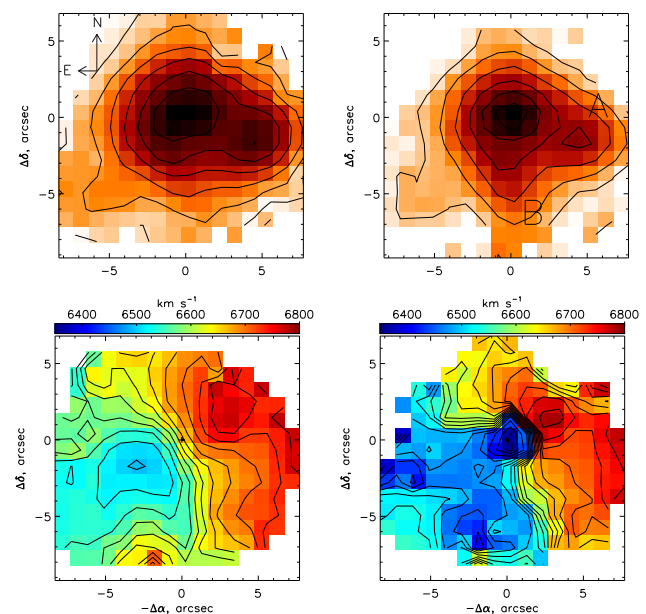


**Figure 1.** Images (top) and velocity fields (bottom) in the H $\alpha$  (left) and [OIII] $\lambda\lambda 4959, 5007$  (right) emission lines according to MPFS data. Regions ‘A’ and ‘B’ are marked.

to convert counts into absolute fluxes. Observations were made successively in two spectral intervals (see Table 1). The overlap of the two spectral domains allowed us to join them so as to operate with a single data cube covering a  $\lambda\lambda 3740 - 7220$  Å spectral range.

To construct the stellar velocity field, we use the cross-correlation technique adapted for MPFS data (Moiseev 2001). Spectra from MILES library (Sánchez-Blázquez et al. 2006) smoothed to the instrumental resolution were adapted as templates for cross-correlation. We have mapped the line-of-sight velocity and brightness distribution fields for the main emission lines using the Gaussian fitting of their profiles. Underlying absorption lines were taken in account as approximation by a linear combination of smoothed and red-shifted MILES templates.

### 2.2 SCORPIO

SCORPIO universal instrument (Afanasiev & Moiseev 2005) allows various spectroscopic and photometric observations to be performed within 6 arcmin field of view. Below we describe each of the modes employed in detail.

### 2.2.1 Fabry–Pérot Interferometer

We used the scanning FPI operating in the H $\alpha$  emission line to study the kinematics of the ionized gas. During the observations we successively took 32 interference images of the object by changing the FPI plate gap. A detailed description of the technique of observations and data reduction can be found in the papers by Moiseev (2002) and Moiseev & Egorov (2008). This reduction yields a data cube, where a 32-channel spectrum with a sampling step of 0.9 Å is attached to each 0.28 arcsec pixel. The spectroscopic resolution is 2.8 Å. The velocity field of the ionized gas and images in the H $\alpha$  emission line were mapped using Gaussian fitting of the emission-line profiles. We also generated an image of the galaxy in the continuum close to the emission line.

We calibrated the emission-line flux map into absolute energy units ( $\text{erg s}^{-1} \text{cm}^{-2}$ ) by comparing it with the H $\alpha$  distribution according to the MPFS data for the central region. The total H $\alpha$ -luminosity of the galaxy was found to be  $2.3 \times 10^{41} \text{ erg s}^{-1}$  given the adopted extinction of  $A_R = 1.5^m$ . The extinction estimate is based on the H $\alpha$ /H $\beta$  line intensity ratio for the HII region to the west of the nucleus (hereinafter referred to as ‘Region A’). According to Kennicutt (1998a), such a luminosity corresponds to star-formation rate of  $\text{SFR} = 18 M_\odot/\text{yr}$ , if we neglect a contribution from the AGN in the H $\alpha$  flux.

### 2.2.2 Direct Images

We took images of the galaxy in the Johnson–Cousins  $V$  and  $R$  bands with a sampling of 0.35 arcsec per pixel. Non-photometric weather conditions prevented the use of standard stars to calibrate fluxes. We performed a coarse calibration in the  $V$  band based on the aperture photometry data listed in the HyperLeda database (<http://leda.univ-lyon1.fr/>). An accuracy of the zero-point is 0.1–0.2 mag. We calibrated the  $R$  image assuming that the average colour index in the disk of Mrk 334 corresponds to that of a normal Sb-Sc-type galaxy:  $(V-R) \approx 0.5$ . The assumption of the normal  $V-R$  color is justified by the known normal 2MASS infrared colours of Mrk 334. The depth of the surface-brightness measurements reaches  $25.5 \text{ mag arcsec}^{-2}$  in the  $V$  and  $R$  bands, which is significantly deeper than the other known images of Mrk 334.

## 3 MORPHOLOGICAL FEATURES OF MRK 334

### 3.1 Line and Continuum Images

We use the MPFS spectra to construct the maps in various emission lines covering the  $7 \times 7 \text{ kpc}$  central region of Mrk 334 (see Fig. 1). The maps show some other bright regions besides the nucleus. The brightest of them, the Region ‘A’, is located 4 arcsec to the west of the nucleus. Gonzalez Delgado et al. (1997) were the first to find it in H $\alpha$ . At our maps it can be seen in other emission lines and in the continuum. Fainter Region ‘B’ is located  $r = 3-4 \text{ arcsec}$  to the south of the nucleus and shows up mostly only in the [OIII] $\lambda\lambda 4959, 5007$  doublet. The continuum image exhibits, in addition to Region ‘A’, an amorphous structure that we refer to as Region ‘C’.

**Table 2.** Parameters of the Photometric Decomposition.

Component	parameter	$V$ filter	$R$ filter
Sersic’s bulge	$n$	2	2
	$\mu_{eff}$	20.3 mag	19.8 mag
	$r_0$	3''2 (1.4 kpc)	3''2 (1.4 kpc)
Inner disk	$\mu_0$	21.5 mag	20.9 mag
	$h$	7''8 (3.5 kpc)	8''7 (3.9 kpc)
Outer disk	$\mu_0$	24.8 mag	24.2 mag
	$h$	32'' (14 kpc)	43'' (19 kpc)

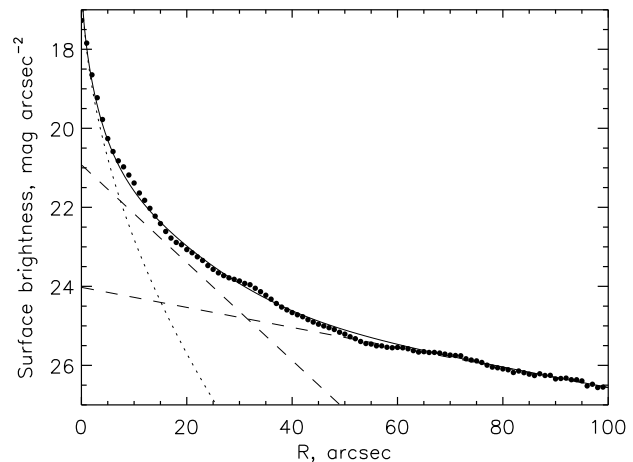


**Figure 4.** The mean  $R$ -band brightness profile (the bold dots) and its model fit (the solid line). The dashed lines show the contribution of each of the disks. The dotted line marks the bulge.

Many authors (see Introduction) believed Mrk 334 to be an interacting system. Their conclusion was based mostly on the presence of an asymmetric spiral arm to the east of the nucleus resembling a tidal tail (Hunt et al. 1997; Rothberg & Joseph 2004). This feature is clearly visible on the FPI continuum image and is absent in the H $\alpha$  line map (Fig. 2). Therefore, this arm does not harbor star-forming regions.

### 3.2 Multicomponent Structure of the Disk and Outer Filaments

The deep images of the galaxy show that the tidal arm noted above is the brightest part of the vast system of shells and lower surface brightness filaments (Fig. 3). The shells have sharp outer edges located about 70 arcsec northwest and about 100 arcsec southwest of the nucleus, which corresponds to 31 and 44 kpc, respectively. The  $R$  band surface brightness of the outer regions is about  $24-25 \text{ mag arcsec}^{-2}$ . Similar arc-like features are typical of galaxies currently interacting or having interacted in the past with a companion (Schweizer & Seitzer 1988; Wehner & Gallagher 2005).

To study the brightness distribution in the filaments, we must remove the axisymmetric components of the galaxy – the bulge and the disk. To decompose the image into components, we use an iterative method of constructing one- and two-dimensional models (Moiseev et al. 2004; Cioi et al. 2005). The idea of the method is to determine the param-

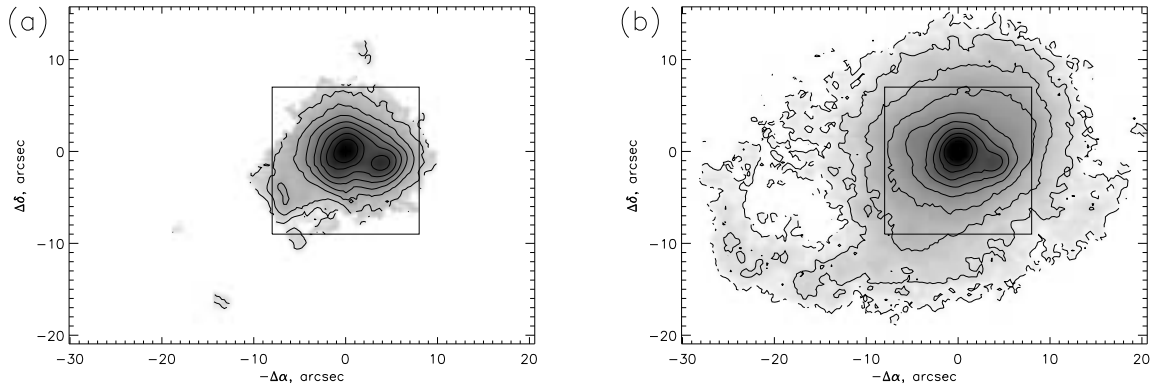


**Figure 2.** FPI images of Mrk 334 in the  $H\alpha$  line (a) and in the continuum (b). The square indicates the region observed with the MPFS

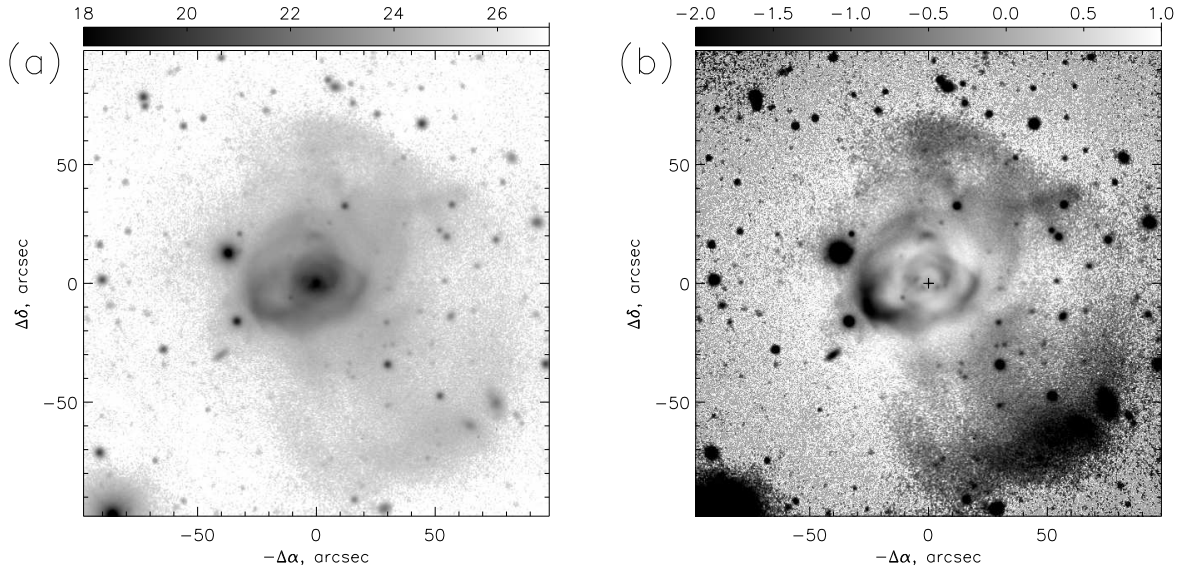


**Figure 3.**  $R$ -band image of the galaxy taken with the 6-m telescope (a) and a residual image after the subtraction of the two-dimensional model (b). The scale is in  $\text{mag arcsec}^{-2}$ .

eters of the exponential disk from the outer parts of the azimuthally averaged brightness profile and subtract the resulting brightness distribution from the original image. The residual image is averaged over round apertures and fitted to the Sérsic's profile for the bulge. We then subtract the bulge model from the initial image and use the residual image to build the next iteration for the disk. When constructing the model we masked the high-contrast features like stars and tidal spirals. We found the galaxy image to be best approximated by the model consisting of a bulge and two exponential disks with different radial scales. Table 2 lists the parameters of the photometric components. Here  $n$ ,  $r_e$ , and  $\mu_{eff}$  are the exponent, effective radius, and brightness of the bulge, respectively, and  $\mu_0$  and  $h$  are the central surface brightness and radial disk scalelength. The position angle and the apparent ellipticity of the disks were fixed in accordance with the orientation of the ionized-gas

disk (Section 5). The results of decomposition performed in the two filters agree fairly well with each other, except that the scalelength of the outer disk is larger by a factor of 1.3 in the  $R$  band.

Figure 4 shows the surface-brightness profile computed by averaging the brightness over elliptical rings. It shows a well-defined break at  $r = 50 - 60$  arcsec and is dominated by the outer disk at larger galactocentric distances. Such multicomponent (two-tiered) disks have now become increasingly popular among the researchers. According to the classification proposed by Erwin et al. (2005), Mrk 334 exhibits a typical type III (antitruncated) surface-brightness profile. Among the galaxies studied by Erwin et al. (2005) such profile characterizes mostly post-interacting objects. A detailed study of individual galaxies also suggests that interaction events may result in the formation of multi-tiered disks. Examples include NGC 615 (Sil'chenko et al.

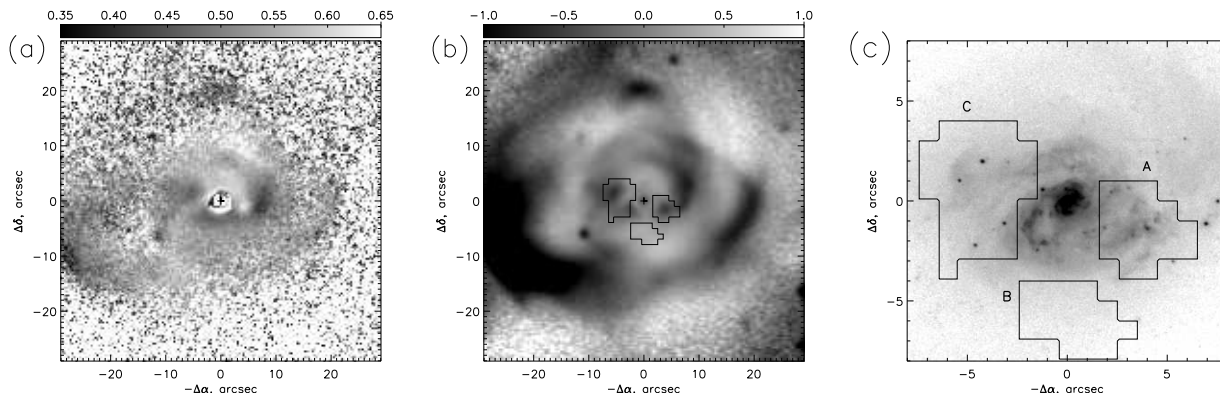


**Figure 5.** The distribution of the  $(V - R)$  colour index in the inner regions of the galaxy (a); residual brightness distribution for the same region (b), and the HST/WFPC2 archive image in the F606W filter (c). The contours in figures (b) and (c) show the boundaries of the condensations identified via MPFS observations.

2001), Mrk 315 (Ciroi et al. 2005), NGC 7217 and NGC 7742 (Sil’chenko & Moiseev 2006).

Mrk 334 appears to represent configuration, where the debris of the companion torn apart by the tidal forces precess in the plane of the galaxy. The outer disk is being formed right now with a relatively long scalelength and a low central brightness. Indeed the parameters of the inner disk (Table 2) are typical for a spiral galaxy, whereas the outer disk has a rather long radial scalelength and the  $\mu_0$  that is typical for low surface brightness (LSB) galaxies. In Mrk334 we caught an LSB disk in the process of formation. Here the mean brightness profile has already become close to an exponential, despite the asymmetry of azimuthal light distribution that is still very inhomogeneous. The brightness of the outer disk should become more homogeneous after a few revolutions that is after about 0.5 – 1 Gyr.

Figure 3b shows the  $R$ -band brightness distribution after subtracting the model consisting of two disks and a bulge. A complex system of bright loops becomes immediately visible. Three characteristic radial scales can be identified: the circumnuclear ring with a radius of about (4 – 5 kpc); inner filaments at a distance of  $r = 9 - 13$  kpc, and outer features — a loop and an arc located northwest and southwest of the nucleus, respectively, which can be observed beyond  $r \sim 40$  kpc. This subdivision of tidal features is rather arbitrary, we are most probably observing a disruption of a single galaxy torn apart by tidal forces and spread along its orbit around Mrk 334. The bulk of the companion stars is concentrated in the central region, because the mean brightness of the inner and circumnuclear filaments is twice higher than that of the outer ones.

The total luminosity contribution of all inner and outer filaments determined after subtracting the two-dimensional model is 30% in the  $V$  and 25% in the  $R$  band. Under the assumption that all filaments (including the circumnuclear ones) were formed by stars of the satellite, we have derived the mass ratio for the galaxies before interaction ranging from 1/5 to 1/3 for the equal  $M/L$  ratios in both galaxies. The scatter of the estimates is mostly due to the uncertain fraction of companion stars dropped into the outer disk. This ratio is close to the conventional boundary between minor and major merging. Whereas in the former case the

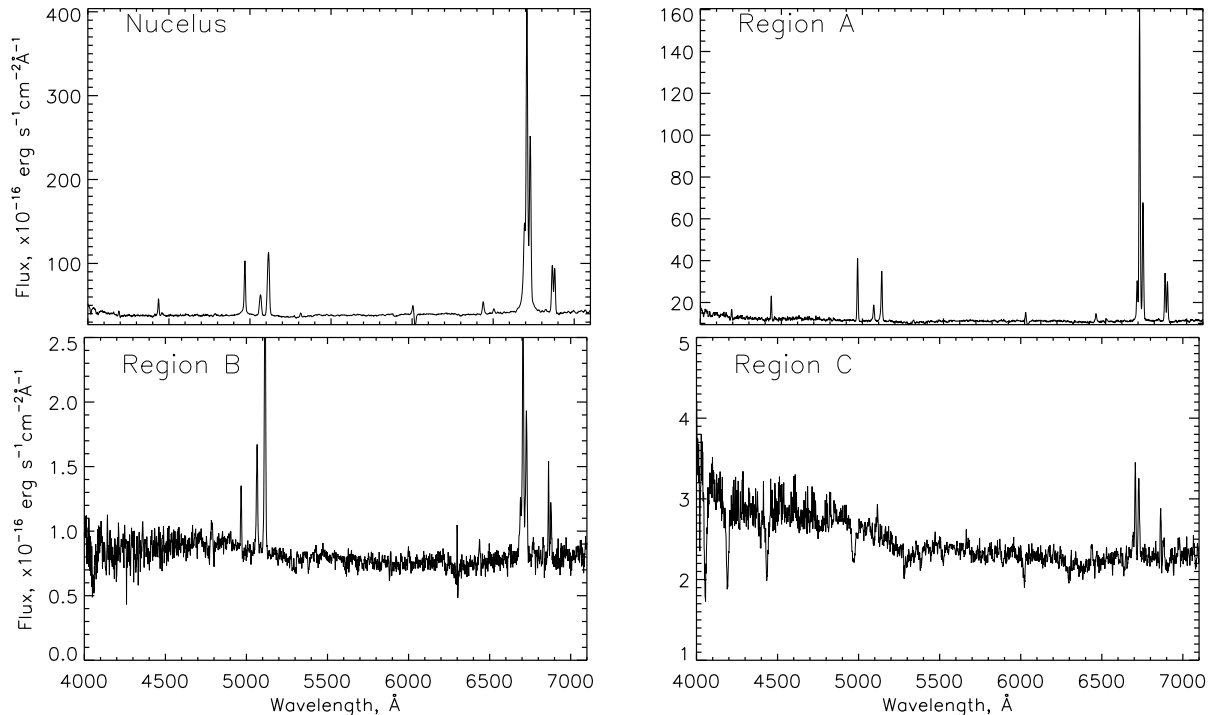
interaction should rather be regarded as a simple accretion of a low-mass companion by the primary galaxy, in the case of major merging this process also distorts appreciably the structure of the more massive companion.

Figure 5 shows the central part of Mrk 334. The system of arcs and loops corresponding to the orbit of the disrupted companion shows up conspicuously on the map of residual brightness. According to the  $(V - R)$  maps, individual fragments of these loops stand out because of their bluer colours, which are indicative of the presence of younger population that may have formed in the process of interaction between the galaxies. The red colour of Region ‘A’ is evidently due to the  $H\alpha$  emission falls within the  $R$ -filter passband. Note that the tidal structures at  $r = 5 - 10$  arcsec are most likely located outside the plane of the galaxy, as follows from the analysis of the gas velocity field (Section 5).

At the same time, the circumnuclear spiral at  $r < 5$  arcsec, which shows up on HST images (Fig. 5c) seems to belong to the galaxy disk plane. The authors having reported HST images of Mrk 334 (Martini & Pogge 1999; Martini et al. 2001) have also pointed out the minispiral and chaotic dust features in the circumnuclear region.

#### 4 SOURCES OF GAS IONIZATION.

Figure 6 shows the integrated spectra of Regions ‘A’, ‘B’, and ‘C’ and of the nucleus extracted from the MPFS data cube. The boundaries of these regions are shown in Figure 5. The spectra of the nucleus and of the knot ‘A’ have much in common: both exhibit strong Balmer lines and weaker forbidden lines, mostly  $[\text{OIII}]\lambda\lambda 4959, 5007$  and  $[\text{OII}]\lambda 3727$ . Region ‘B’ shows the opposite pattern: the most conspicuous line is  $[\text{OIII}]\lambda 5007$ , which is even brighter than  $H\alpha$ . The spectrum of Region ‘C’ exhibits, along with a very weak  $H\alpha$  emission, high-contrast MgI, Fe, and Ca and Balmer-line absorptions. Such a spectrum is typical for a composite post-starburst region. We estimate the luminous-weighted age of



**Figure 6.** Integrated spectra of individual regions in Mrk 334.

the stellar population as 1.1-1.6 Gyr using the ULYSS<sup>1</sup> program package.

Regions with different emission-line spectra must also differ in their ionization sources. We construct the diagnostic diagrams to determine the ionization mechanism for the inner regions of the galaxy. Given the line ratios for different excitation mechanisms, we can identify regions dominated by thermal (young stars), nonthermal (active nucleus), or shock ionization (hereinafter referred to as HII, AGN, and LINER). Figure 7 shows the most typical diagrams. In the diagrams we adopted the boundaries separating domains corresponding to the different excitation mechanisms from Veilleux & Osterbrock (1987). We ignored the effect of internal extinction, because we use the intensity ratios of the lines with close wavelengths.

Mrk 334 is classified as a Sy 1.8-type galaxy and its Balmer-line profiles have a low-contrast broad component. We decomposed the H $\alpha$  and H $\beta$  line profiles into two Gaussian functions: one for the broad and one for the narrow component. Only the narrow component flux was used in the diagnostic diagrams.

The points in the diagrams of Fig. 7 show the line ratios in each MPFS spaxel. In all diagrams the points corresponding to the nucleus lie at the HII-LINER boundary. Here the main ionization mechanisms are radiation of young stars and shocks, and not the nonthermal UV continuum as it is typical of an active nucleus. The points corresponding to the nucleus are located in the diagrams so far from the LINER-AGN boundary that the nucleus of Mrk 334 should be clas-

sified as a LINER rather than a Sy galaxy. This conclusion is consistent with the recent spectrophotometric studies of the nucleus reported by Lumsden et al. (2001). The asterisks in Fig. 7 indicate the line ratios in the nucleus as inferred from their long-slit spectrum<sup>2</sup>. Figure 7 demonstrates the good agreement between their data and our measurements for the nucleus except for the [SII]/H $\alpha$  ratio. The last discrepancy must be due to the fact that we corrected our spectra for the atmospheric absorption band which partially overlaps with the [SII] lines and decreases sulfur flux by  $\sim 0.1$  dex. Lumsden et al. (2001) say nothing about applying such a correction.

The emission-line ratios observed in the nucleus can be explained in terms of the following supposition. The star formation in the nucleus is so violent that the total line emission is determined mostly by the collective effect of photoionizing radiation of young stars and by the shocks produced by supernova explosions. At the same time, the emission lines of the active nucleus are barely visible against the circumnuclear starburst. The weak broad component with  $FWHM \approx 2500 \text{ km s}^{-1}$  in the hydrogen line profiles and FeII features in the spectrum of the nucleus are the only indications of an AGN central engine.

In all diagrams the points belonging to Knot ‘A’ lie deeply in the region corresponding to the ionization by OB stars radiation. Thus ‘A’ is indeed a region of intense ongoing star formation. It accounts for 15 – 20% of the total H $\alpha$  luminosity, and such a fraction formally corresponds to a star formation rate of  $SFR = 3 M_{\odot}/\text{yr}$ . Such a high value

<sup>1</sup> ULYSS is an open code located at <http://ulyss.univ-lyon1.fr/> and based on the papers of Koleva et al. (2009), Chilingarian et al. (2007) and other.

<sup>2</sup> The fluxes reported by Lumsden et al. (2001) are extinction corrected, but, as we point out above, this correction is negligible for the diagrams

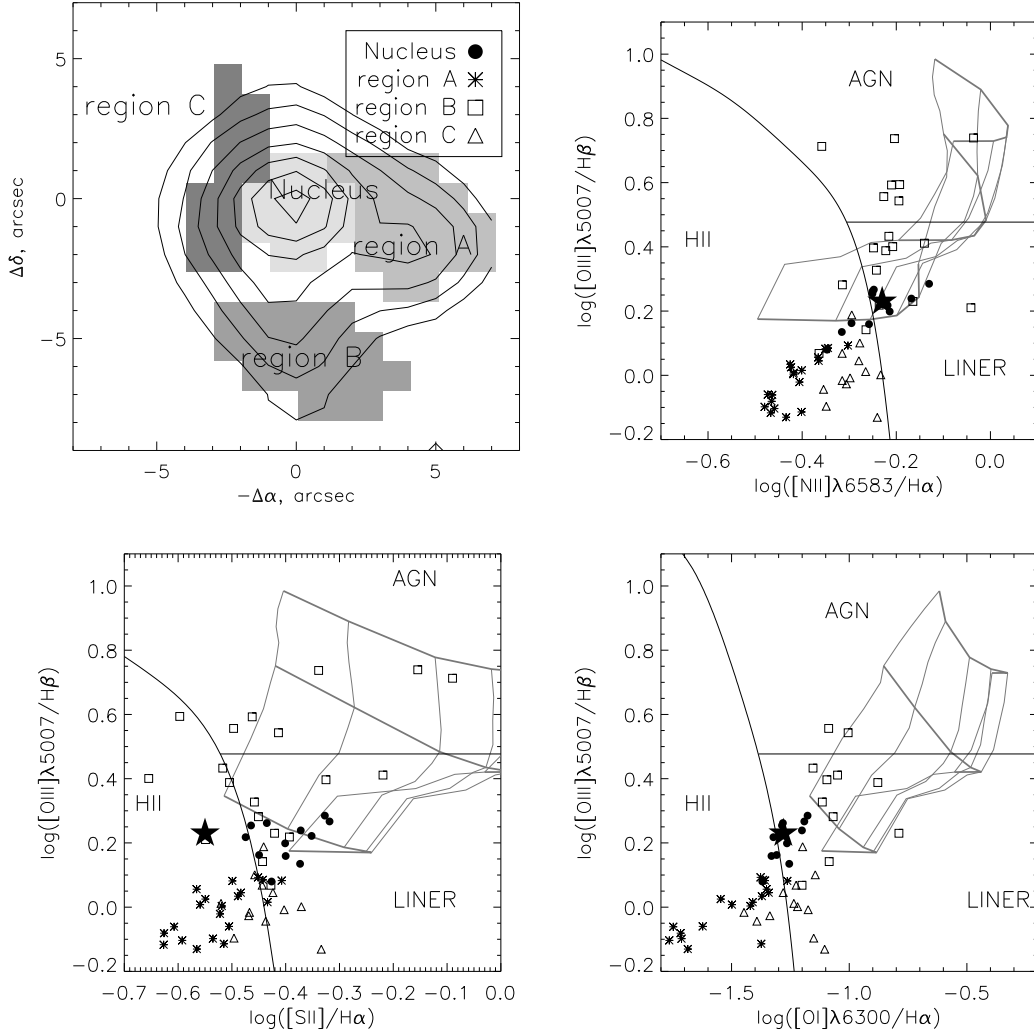


**Figure 7.** The diagnostic diagrams for various regions in Mrk 334. The top left panel shows the mask used to select the galaxy regions, the [OIII]-line isophotes are overlapped. The circles, asterisks, squares, and triangles correspond to the nucleus and Regions ‘A’, ‘B’, and ‘C’, respectively. In the case of Region ‘C’ only spaxel contained emission line spectra are shown. The black star shows the data by Lumsden et al. (2001). The solid black lines separate the domains corresponding to different excitation mechanisms. The gray lines show the grid of shock+precursor models from Allen et al. (2008) for  $n = 1 \text{ cm}^{-3}$  and solar elemental abundances. The thin and bold gray lines mark the contours of constant magnetic parameter  $B/n^{1/2} = 0.1, 0.5, 1.0, 2.0, 5.0, 10 \mu\text{Gcm}^{3/2}$ , and contours of constant velocity,  $v = 250, 350, 450 \text{ km s}^{-1}$  (velocities increase from bottom to top), respectively.

(equivalent to the total SFR in the starburst galaxy M 82) in a relatively compact region (1 kpc in size) is indicative of a powerful starburst.

Condensation ‘B’ appears to be the most intriguing among these features: it exhibits unusually high [OIII]/H $\beta$  line intensity ratios (see Fig. 8a) that formally correspond to the ionization by an AGN. Two hypotheses can be suggested to explain this peculiarity. First, Region ‘B’ may be the active nucleus of the satellite. Barth et al. (2008) recently observed a similar situation in the interacting galaxy NGC 3341, where the spectrum of the nucleus of the disrupted companion exhibits Seyfert-type features. However, Condensation ‘B’ is barely visible on the optical continuum images of Mrk 334. Observations made at the 6 cm wavelength (Ulvestad 1986) with an angular resolution of 0.4–0.6

arcsec also demonstrate the lack of a nonthermal radio emission typical of an active nuclei in Region ‘B’.

The second hypothesis is based on the fact that Region ‘B’ is located close to the tidal arclike structures identified in the circumnuclear region images (Fig. 5b). It would be safe to assume that here we see the intersection between the galaxy disk and the orbit of the disrupted companion remnants. It is the locus where the debris have ‘punched’ the gaseous disk of Mrk 334, thereby creating in Region ‘B’ a cavern with lower than ambient gas density. The high degree of ionization of the gas is due to a powerful shock. This idea is also supported by the electron-density estimates derived from the [SII] $\lambda\lambda 6730/6717$  line flux ratio using the relation adopted from Osterbrock (1989) for  $T_e = 10\,000 \text{ K}$ . The electron density is equal to  $n_e = 250 - 430 \text{ cm}^{-3}$  in the nucleus,  $n_e = 200 - 350 \text{ cm}^{-3}$  in Region ‘A’, and increases

to  $500 \text{ cm}^{-3}$  to the north of this HII region (Fig. 8b). At the same time, the sulphur line ratio is less than 0.7 at almost all points of Condensation ‘B’, which is impossible to interpret in terms of simple photoionization models. It is indicative of high temperature and low gas density ( $n_e < 20 \text{ cm}^{-3}$ ).

We tried to compare the line ratios observed in Region ‘B’ with the results by the modern shock ionization simulations adopted from Allen et al. (2008). We found that the theoretical shock+precursor model predictions describe fairly well the line ratios observed in Region ‘B’ (Fig. 7) for parameters that can be reasonably expected for the interstellar medium: the density of  $1 \text{ cm}^{-3}$ , solar elemental abundances and magnetic-parameter  $B/n^{1/2} = 0.1 - 10 \mu\text{Gcm}^{3/2}$ . The required shock speed is  $250 - 350 \text{ km s}^{-1}$ . The shock origin of the [OIII] emission is also evident from the line broadening. Indeed the width of the [OIII] lines in Region ‘B’, after instrumental width correction, corresponds to the  $\sigma = 160 - 200 \text{ km s}^{-1}$  instead  $60 - 100 \text{ km s}^{-1}$  in other disk points, with the exception of the nucleus. More kinematic evidences will be presented in the next Section.

Region ‘C’ may be satellite debris that has recently punched a hole in the gaseous disk of Mrk 334. It is located close to Region ‘B’; it appears sufficiently bright in the continuum images and its spectrum contains lines of young stellar population; it appears compact compared to other nearby filaments. It may actually be the remnant of the nucleus of a companion galaxy. The data on the ionization sources in this region are rather scarce and available only for the boundary between Region ‘C’ and the nucleus of Mrk 334 because the spectrum shows mostly stellar absorptions. In the diagnostic diagrams Region ‘C’ lies in the HII and LINER sectors. The photoionization is caused here mostly by star-forming processes, and the shock ionization contributes appreciably in the points located close to the nucleus.

## 5 KINEMATICS OF IONIZED GAS AND STARS.

The H $\alpha$  velocity field derived from the FPI data seems to be in a good agreement with the model of a regular rotating thin disk (Fig.9). We fitted the velocity field by the “tilted-ring” model using the algorithms employed earlier to study NGC 6104 (Smirnova et al. 2006). The circular rotation explains the gas velocity field fairly well. Therefore we think that the inner tidal features ( $r = 5 - 10 \text{ arcsec}$ ) are located outside the galaxy plane and do not perturb the entire gaseous disk but only cross it in some places. We found the disk inclination to be  $i_0 = 34 \text{ pm}6 \text{ deg}$  and the line-of-nodes position angle of  $PA_0 = 297 \pm 3 \text{ deg}$ . Fig. 10 shows the rotation curve of ionized gas ( $V_{\text{rot}}$ ) and the radial variations of the kinematic axis ( $PA_{\text{kin}}$ ). The data points in the range of  $r = 12 - 22 \text{ arcsec}$  come from three outer HII regions located far from the central disk:  $PA_{\text{kin}}$  could not be determined from these regions, and we assume it to be equal to the mean  $PA_0$  of the disk.

The same figure shows kinematic parameters for the old stellar population. The rotation velocity measured for stars is about twice (by  $\sim 100 \text{ km s}^{-1}$ ) smaller than that found for the ionized gas. This discrepancy must be due to asymmetric drift, because the central velocity dispersion of stars

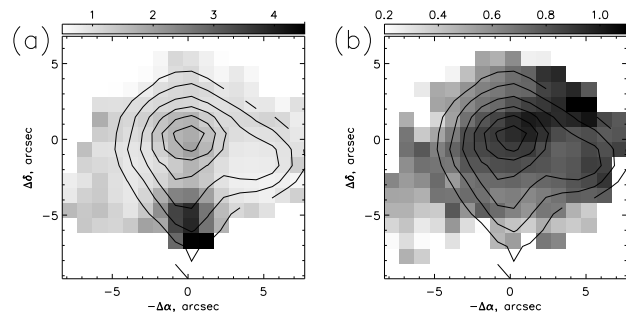


**Figure 8.** Map of the [OIII]λ5007/H $\beta$  (a) and [SII]λ6731/6717 (b) line ratios. The [OIII]λ5007 isophotes are overlapped. In the case of sulphur lines, darker colours correspond to higher electron density.

reaches, according to our estimates,  $170 - 200 \text{ km s}^{-1}$ . The rotation curve of both gas and stars exhibits a characteristic peak near the effective radius of the bulge. At greater galactocentric distances,  $r = 4 - 12 \text{ arcsec}$ , the rotation velocity of gas is almost constant and equal to  $210 - 220 \text{ km s}^{-1}$ . The  $V_{\text{rot}}$  of the external HII regions mentioned above is lower by  $40 - 50 \text{ km s}^{-1}$ , however, we have no grounds to believe that these regions may be located outside the disk of the galaxy. It seems to be more likely that the formal decrease of the rotation velocity results from a contribution of non-circular gas motions.

Small variations of  $PA_{\text{kin}}$  at  $r < 5 \text{ arcsec}$  indicate the influence of the circumnuclear spiral on the kinematics of the gaseous and stellar subsystems. The  $PA_{\text{kin}}$  abruptly deviates from the line of nodes at  $r = 8 - 11 \text{ arcsec}$ . Such a behaviour is indicative of large-scale noncircular motions at the edge of the HII disk. The residual-velocity map (Fig.9b) shows the distribution of observed velocities after the subtraction of the model. Deviations from circular rotation are small ( $15 - 20 \text{ km s}^{-1}$ ) in the regions with the brightest H $\alpha$  emission. However, to the south from the nucleus an extended region can be seen where peculiar velocities are much higher and vary smoothly from  $-70$  to  $+60 \text{ km s}^{-1}$  in the east-west direction. Region ‘B’ is located here, which we have identified earlier by its spectrophotometric properties, primarily by its high [OIII]/H $\beta$  ratio. Now we see that this region is also distinguished by the peculiar kinematics of ionized gas. Such a velocity distribution corroborates the hypothesis — suggested above — that Region ‘B’ is the locus where the debris of the disrupted companion crossed the gaseous disk of the galaxy.

An alternative explanation of the observed gas kinematics is a jet-clouds interaction similar to that observed in Mrk 3 (Capetti et al. 1999) or Mrk 533 (Smirnova et al. 2007). However, this mechanism is unlikely for Mrk 334. Firstly, as we already pointed out above, this galaxy has no extended radio structure. Secondly, if the jet acts on the interstellar medium then the expected gradient of peculiar velocities should be directed away from the nucleus, i.e., in the radial and not in the azimuthal direction as we see in Fig.9b.

The velocity fields derived from the MPFS data (Fig.1) have allowed us to study the kinematics of gas in lines excited by different mechanisms, albeit with lower accuracy and in coarser detail compared to the results based on the



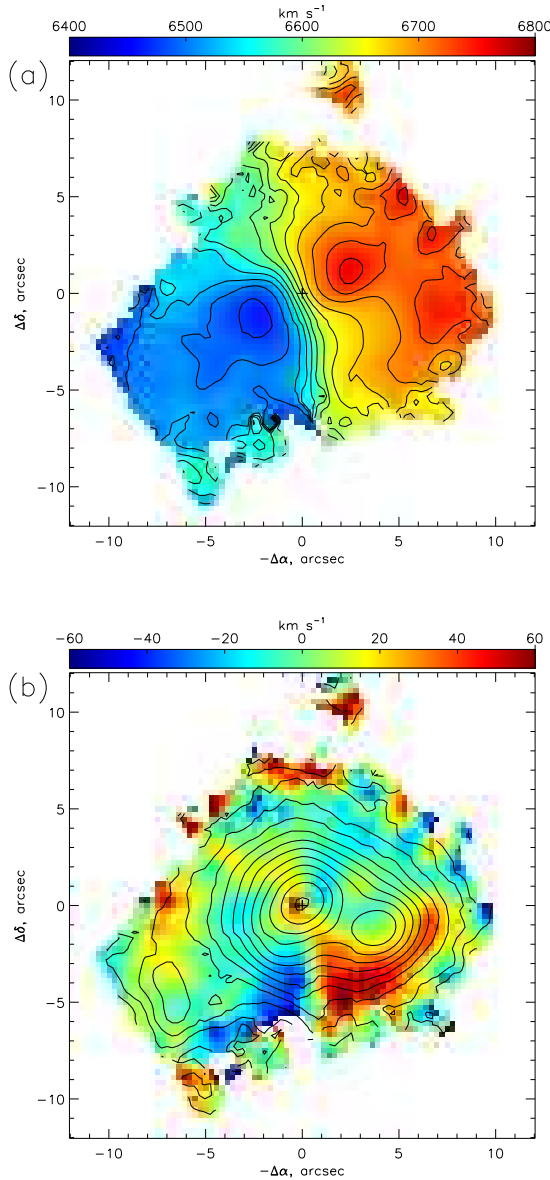


**Figure 9.** Kinematics of ionized gas according to the  $H\alpha$ -line FPI data: the velocity field (a) and the residual velocities (observations minus model) with  $H\alpha$ -line isophotes overlapped (b).

FPI  $H\alpha$  data. The gas motions observed via most of the low-excitation emission lines ([OI], [OII], [NII], [SII]) agree well with the picture found in the  $H\alpha$  line. Namely, they show a circular rotation with appreciable deviations near Region ‘B’. Only the velocity distribution in the [OIII] line differs from the overall pattern (Fig.1, bottom). Figure 11 shows the residual velocities in this line after the subtraction of the circular-rotation model derived from the  $H\alpha$  data. Two features are apparent. First, the residual velocities in Region ‘B’ reach  $-150 \text{ km s}^{-1}$ , which is greater by amplitude than the corresponding velocities for the low-excitation lines. Second, the galaxy nucleus shows a significant excess of negative velocities (down to  $-300 \text{ km s}^{-1}$ ). Similar gas outflows from AGN (excess of ‘blue’ velocities, first and foremost, in the [OIII] line) were found in the integral-field spectroscopy data

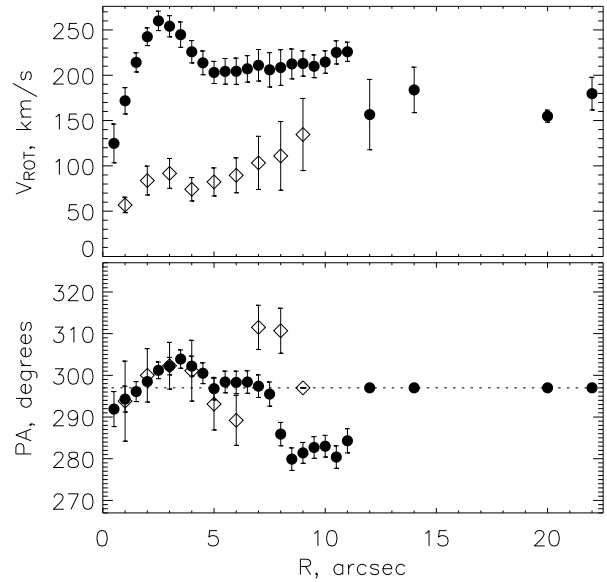


**Figure 10.** The rotation curve (top) and variations of the position angle of the major axis with a radius (bottom). The black circles show the  $H\alpha$ -line FPI velocity-field measurements and diamond signs mark the measurements for the stellar component (MPFS).

for Seyfert galaxies studied by us and by other teams: Mrk 315 (Ciroi et al. 2005), NGC 2273 (Moiseev et al. 2004), NGC 2992 (García-Lorenzo, Arribas & Mediavilla 2001), NGC 6104 (Smirnova et al. 2006) and others. A nuclear-blueshifted outflow associated with this feature is usually interpreted as a jet-clouds interaction (Ferruit 2002), or, in a more general case, as hot wind emerging from an active nucleus (Komossa et al. (2008) and references therein). However, the situation in Mrk 334 must be different. Firstly, no radio jet can be seen in high-resolution radio maps, in any case, its size cannot exceed 0.5 arcsec. Secondly, in the nucleus itself the contribution from the nonthermal component to the ionization of gas is smaller than that of star formation (see Section 4). Thirdly, unlike the examples of active galaxies mentioned above, the high-velocity outflow in Mrk 334 is observed only in the [OIII] line. This outflow is most likely associated with intense star formation in the nucleus rather than with the central engine itself. Thus, what we observe in the [OIII] line is a low-density gas ejected above the plane of the galaxy as a result of multiple supernova explosions – the so-called ‘superwind’. Below we analyse this possibility in more detail.

We computed the velocity field of the stellar component by correlating the spectra of the galaxy with the stellar spectra from the MILES library and selecting the spectral type of the template and wavelength interval so as to maximise the amplitude of the cross-correlation function. Figure 11 shows the velocity field corresponding to the old stellar population determined by cross-correlation of the galactic spectra with the spectrum of a K0III type star in the interval of  $\lambda 5120 - 5800 \text{ \AA}$ . This velocity field was used to construct the stellar rotation curve presented in Fig. 10. However, a

significant contribution of younger stellar population can be seen in the bluer part of the galaxy spectra in some regions. Thus in the wavelength interval  $\lambda 3750 - 4350\text{\AA}$  the coefficient of correlation with the spectrum of a F-type star exceeds the corresponding value for a K-type star in the  $\lambda 5100 - 5500\text{\AA}$  wavelength interval. The measurements made for the ‘old’ and ‘young’ populations yield different line-of-sight velocities. Figure 11 shows the difference between the velocity fields of old and young stars. In the nucleus the difference is small and does not exceed  $20\text{ km s}^{-1}$ , which is comparable to measurement errors. However, the velocity difference reaches  $-80\text{ km s}^{-1}$  in two regions to the east of the nucleus. Both regions identified in the field of stellar residual velocities coincide with the inner tidal loops in the circumnuclear region, including Region ‘C’, (Fig. 5b). These facts lead us to suggest that here we see two kinematic components along the same line of sight. The old stellar population belongs to the disk of Mrk 334 and exhibits normal circular rotation. At the same time, the tidal filaments formed in the process of the companion disruption are dominated by younger population (as a result of a relatively recent burst of star formation). The filaments are located outside the disk plane as is evident from their line-of-sight velocities. Fig. 11c also shows another region with significant negative differences of the young and old stars velocities to the west from the nucleus. It may also include stars from the companion galaxy.

An interesting pattern emerges if we cross-correlate the spectra in the NaD doublet spectral domain. Figure 11 shows the line-of-sight velocities for this line measured after the subtraction of the velocity field of the old stellar component. An excess of negative residual velocities up to  $-180\text{ km s}^{-1}$  is immediately apparent in the nucleus of the galaxy. The NaD line is present not only in the spectra of late-type stars but also in the spectra of the interstellar medium. It is reasonable to associate the excess velocities in this line with the same superwind that we found in the [OIII]-line data for the ionized gas. We should note that outflow velocities may be underestimated because the contamination of the NaI line by absorption from the stellar population is also present.

## 6 X-RAY RADIATION OF MRK 334

Let us now briefly discuss the peculiarities of the distribution of X-ray flux of Mrk 334 according to the *ROSAT* data. Zimmermann et al. (2001) report isophotes of the smoothed image in the energy interval of  $0.1 - 2.4\text{ keV}$ . The X-ray source with the luminosity of  $L_X = 2.6 \cdot 10^{42}\text{ erg s}^{-1}$  is unambiguously identified with the galaxy. However, the contours of the X-ray image are appreciably offset with respect to the optical nucleus, and outer isophotes coincide with the tidal structures at  $r = 70 - 100\text{ arcsec}$  northwest and southwest of the centre of the galaxy (Fig. 12). Hence the diffuse X-ray emission is associated with the merging galaxy system but not with the Seyfert nucleus. Especially striking is the almost exact coincidence of the outer X-ray isophotes with the edges of optical filaments which is surprising given the relatively low spatial resolution of the *ROSAT* data.

If the most of the X-ray radiation of Mrk 334 is unassociated with the active nucleus, it may be due either to unre-

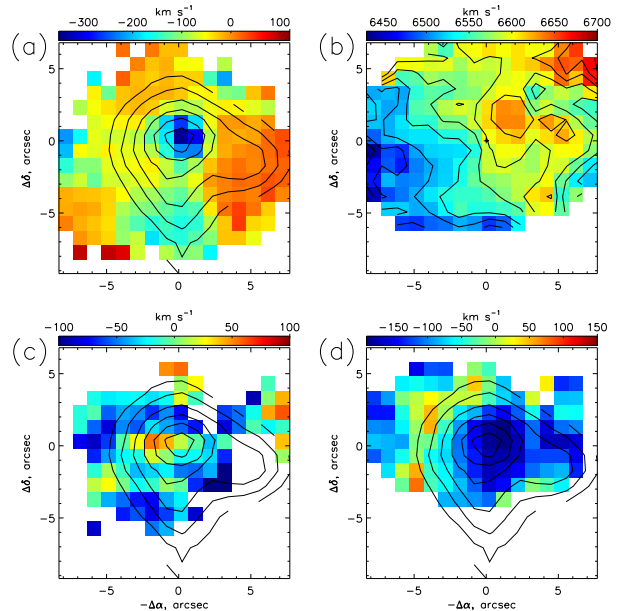


**Figure 11.** (a) Residual [OIII]-line velocities (observed velocities minus the rotation model in  $H\alpha$ ). (b) – Velocity field of the old stellar population. (c) – The difference between the velocities of the ‘young’ (F-type stars) and ‘old’ (K-type stars) populations. (d) – The residual velocities in the NaD line minus the rotation velocity of the old stellar population. Figures (a), (c), and (d) are shown with the [OIII]-line isophotes superimposed.

solved stellar sources or to the outer hot gas. We believe the former variant to be unlikely. Excess number of X-ray point sources – close binaries, ULXS, young supernova remnants associated with a starburst – are observed in a number of interacting galaxies. In this case other signs of ongoing star formation and, in particular, HII regions, should also be apparent at the periphery of the galaxy. However, according to our data,  $H\alpha$  emission is concentrated only in the central region, inside  $r < 12\text{ arcsec}$ .

If the source of the emission is hot gas then where does it come from? It cannot be the corona of the disrupted companion like those observed in giant elliptical galaxies, because the mass of the companion is not too large, and Mrk 334 is a disk galaxy. An HI corona may have formed from the gas scattered as a result of interaction, whereas most of this gas is concentrated in the disk plane. It is, however, unclear how this gas can be heated.

We could suggest only one more or less realistic scenario to explain the formation of the extended X-ray structure. The inner parts of the galaxy are marked by high star-formation rate. Our estimates yield  $\text{SFR} = 18\text{ M}_\odot\text{ yr}^{-1}$  (from the  $H\alpha$  line) and  $12\text{ M}_\odot\text{ yr}^{-1}$  (as inferred from the *IRAS* FIR using the relations from Kennicutt (1998b)). Such an intense star-forming activity in a compact region accompanied by supernova explosions may give rise to a superwind phenomenon that results manifests significant heating of the interstellar medium and its outflow within a wide cone perpendicular to the galaxy disk (Heckman, Armus & Miley 1990; Veilleux, Cecil & Bland-Hawthorn 2005). Inside the cone the temperature may rise to  $10^7\text{ K}$ , and hence the gas should be a powerful X-ray source. The starburst starts early enough during the interaction of galaxies — it begins be-

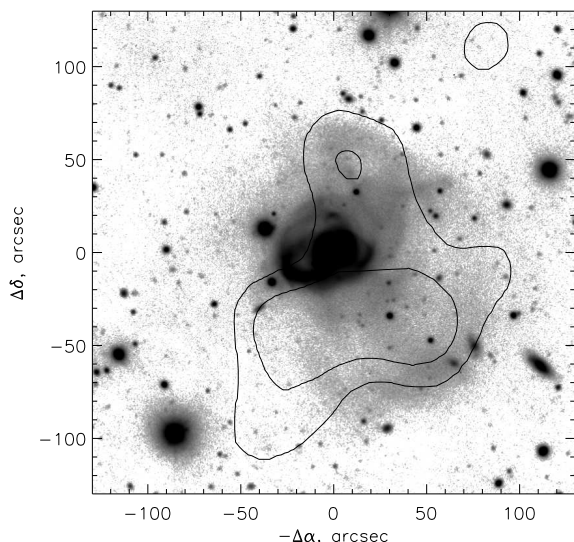


**Figure 12.** The *R*-band image of the galaxy with *ROSAT* X-ray isophotes from Zimmermann et al. (2001) superimposed.

fore the complete disruption and merger of the companion. As an example, we can mention the well-known superwind galaxy M 82 that is currently in the process of a tidal interaction with M 81, or the NGC 6285/6286 galaxy pair (Shalyapina et al. 2004). Thus, a hot gaseous ‘bubble’ or cone could be formed above the plane of Mrk 334 even before the final stage of the merging. The spatial distribution of the hot gas was then distorted because of the significant perturbations of the gravitational potential of the system. We observe the result of these distortions as the offset of the X-ray brightness centre in the sky-plane projection.

We have already pointed out in Section 5 that the MPFS spectra are indicative of the presence of the superwind in Mrk 334. Gas motions directed toward the observer have been found in the central region. The observed velocities ( $180\text{--}300\text{ km s}^{-1}$ ) are typical of superwind galaxies with intense star formation in their nuclei (Veilleux et al. 2005).

## 7 DISCUSSION.

The analysis of various observational data lead us to conclude that Mrk 334 is in the process of merging with a companion that has already been almost completely disrupted by the tidal forces. Is the nuclear activity associated with such a close interaction? Let us first turn to the galaxy morphology. The inner region ( $r \leq 3\text{ kpc}$ ) hosts a well-defined spiral pattern (Fig. 5c). Nuclear spirals in Mrk 334, where sites of star formation are located, are relatively brighter than similar features in other galaxies (Deo et al. 2006). The luminous HII Region ‘A’ located in the western spiral arm has the size typical of giant star-forming complexes in nearby spiral galaxies. Infrared and UV observations (Muñoz Marín et al. 2007; Rothberg & Joseph 2004) confirm that Mrk 334 is a starburst galaxy. This explains why in the ionization diagrams the part of the data points

that belong to the nucleus lie in the domain corresponding to the ionization by young stars.

Such a powerful burst of star formation in a rather compact region produces a hot gas superwind. Low-density gas heated by frequent supernova explosions forces its way through the dense and cold gas of the disk to form a wide-cone outflow in the direction perpendicular to the galaxy plane. Superwind is usually most conspicuous in edge-on galaxies with the cone of hot gas fully open toward the observer. However, Mrk 334 has a less convenient orientation and the cone is seen projected against the bright disk of the galaxy and hence the conclusions about the presence of a superwind are to be based on the circumstantial evidences. Firstly, negative [OIII]-line velocities are observed toward the nucleus of the galaxy (the base of the outflow) suggesting outward motions of highly ionized gas with velocities of  $200\text{--}300\text{ km s}^{-1}$  perpendicular to the galactic plane. Also, the  $150\text{--}180\text{ km s}^{-1}$  motions are observed in the NaD absorption line. The velocities are larger in the high-excited gas than in neutral medium, which is typical for galactic winds (Veilleux et al. 2005).

A second indication of the superwind is provided by the observed asymmetry of the X-ray flux distribution with respect to the nucleus.

Interaction-related processes become important as close to the nucleus as at the distances of  $1\text{--}2\text{ kpc}$  from it. We see their footprints as Regions ‘B’ and ‘C’ and a system of tidal arcs and envelopes extending out to galactocentric distances of  $40\text{ kpc}$ . Fig. 13 shows schematically the inner region of the galaxy. An analysis of the kinematics of gas and stars led us to conclude that the orbits of the debris of the disrupted companion lie outside the disk of Mrk 334 and cross it at a considerable inclination. In the region of this cross-point we observe a cavern with gas density lower than that of the ambient surrounding medium (Region ‘B’) which has formed as a result of the crossing of the disk by a dense stellar condensation. The rotation velocity at this location is  $200\text{--}250\text{ km s}^{-1}$ , implying that the fragments of the companion also move with the velocities of the same order relative to the gaseous disk. Also, we find evidence of a high velocity collision in the gas kinematics and ionization. The collision has strongly perturbed the velocity field in the  $\sim 3\text{ kpc}$  size region. The maximum amplitude of the line-of-sight velocity perturbations amounts to  $70\text{ km s}^{-1}$  in low-excitation lines and reaches  $150\text{ km s}^{-1}$  in the [OIII], because in this line we see low-density gas ionized by a powerful shock. The ionization state in Region ‘B’ can be described in terms of the shock+precursor model for a shock propagating at a speed of  $250\text{--}350\text{ km s}^{-1}$ . The mutual agreement of all the three estimates for the collision velocity supports the adopted interpretation of the formation of Region ‘B’.

Unfortunately, in the literature we have not found any detailed simulations of the gaseous disk response to the intrusion of a self-gravitating body whose mass is small compared to that of the entire galaxy. As a close analogy, we can mention the paper by Levy (2000), that briefly analysed the response of a gaseous disk of a galaxy to the crossing by a globular cluster. Even in such a relatively small-scale collision the resulting shock propagates to at least five to six vertical disk scale heights.

We believe that the remnant of the companion galaxy now observed as Region ‘C’ is the most likely candidate ob-

ject to have punched the disk of Mrk 334 and produced there a cavern of hot gas. The line-of-sight velocities of the stellar population associated with Region ‘C’ differ appreciably (by almost  $100 \text{ km s}^{-1}$ ) from the velocities of the old stellar population in the galactic disk. How is Region ‘C’ located with respect to the observer? Residual velocities of ionized gas in the cavern (Region ‘B’) are mostly negative. This means that the body that produced the cavern crossed the disk plane moving toward us and must now be located above the galaxy disk with respect to the observer (Fig. 13). Residual velocities of the young stellar population in Region ‘C’ are also negative implying that the nucleus of the companion traversed less than a quarter of its orbit after the collision. In accordance with the rotation curve we estimate the dynamical age of the cavern in Region ‘B’ as  $t \leq 10^7$  yr. Therefore, we indeed deal with a recent collision and the cavern has not yet cooled down or condensed.

Our photometric analysis of the tidal filaments yields a mass ratio for the interacting galaxies ranging from 1/5 to 1/3. The merger must have occurred between two gas-rich galaxies. Indeed, the total luminosity of nonaxisymmetric features in the optical images is 25 – 30% of the total luminosity of the galaxy. Hopkins et al. (2008) suggest that the ‘excess flux’ is even greater in the K band where its contribution amounts to 45%. According to Hopkins et al. (2008), such a high percentage of the excess flux can be reproduced in the model of gas-rich galaxies merging, and the process results in the formation of a LIRG galaxy, just as in the case of Mrk 334.

In Mrk 334 we appear to observe a transition from the LIRG stage to the phase of nuclear activity. The fact that the activity of the nucleus of the galaxy has started only recently is proved by weak water-ice absorptions in the infrared spectra that are indicative of a certain well-defined phase in the evolution of the object (Spoon et al. 2002).

Thus, both the burst of star formation and nuclear activity in Mrk 334 date back to a rather recent epoch and their age is comparable to the dynamic time scale of the interaction. Li et al. (2002) pointed out, by references to Yuan et al. (in preparation), that ULIRGs experienced the stage of ‘diffuse merger’ when the nuclei of the interacting galaxies already merge together but have not yet formed a single nucleus. Composite activity — active nucleus + star formation — intensifies abruptly during this stage, and this appears to be now the case in Mrk 334.

## 8 CONCLUSIONS.

We used 3D spectroscopic data and deep images to explore the structure and kinematics of the galaxy Mrk 334. The galaxy has a composite (AGN+starburst) nucleus and extended tidal structures in the form of loops and arcs observed at galactocentric distances ranging from 2 to 40 kpc. Extensive spectroscopic and photometric data allowed us to thoroughly analyse the structure of the inner regions of the galaxy. We consider the following points to be the most important:

(i) The main galaxy-to-companion mass ratio is about 3 to 5. The average surface-brightness profile shows a multi-tired structure and can be decomposed into a bulge and two exponential disks. We caught the galaxy in the process of

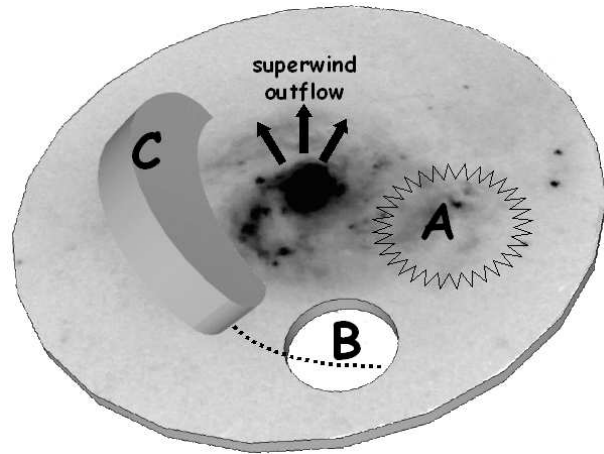


**Figure 13.** Sketch of the proposed model describing the spatial structure of the inner ( $r < 5$  kpc) region of Mrk 334. The *HST* image from Fig. 5 is projected onto the plane of the galactic disk

the formation of an outer low-surface-brightness disk from the debris of the disrupted companion.

(ii) The central region of the galaxy demonstrates a powerful starburst that must have been triggered by the galaxy merger. Circumnuclear star formation is so intense that its contribution to the total ionization of gas exceeds that of the active nucleus. As a result, the corresponding data points in the diagnostic diagrams lie in the HII/LINER domain. Such a powerful burst of star formation in a compact region gives rise to a superwind with velocities of  $200 - 300 \text{ km s}^{-1}$ . The asymmetric X-ray brightness distribution on *ROSAT* maps is consistent with this hypothesis.

(iii) We revealed a region  $\sim 2$  kpc east of the centre that is possibly the nucleus of a disrupted companion. The spectrum of this region exhibits stellar absorptions that are typical of a region that has undergone a burst of star formation about one Gyr ago. The radial velocities of the stars located in this region differ appreciably from the stellar disk of Mrk 334 onto which it is projected. In the disk of the galaxy we found a cavern filled with low-density ionized gas. We interpret this region as a site of a recent (about 10 Myr ago) crossing of the gaseous disk by the remnants of the disrupted companion. This supposition allows us to explain the unusually high  $[\text{OIII}]/\text{H}\beta$  line ratio observed in this region that can be produced by a powerful shock propagating with a velocity of more than  $250 \text{ km s}^{-1}$ . The non-circular gas motions in this region agree with the crossing of the galaxy disk by the debris of the companion.

This work is based on observations made with the 6-m telescope of the Special Astrophysical Observatory of the Russian Academy of Sciences operated under the financial support of the Ministry of Science of the Russian Federation (Registration Number 01-43). This research has made use of the NASA/IPAC Extragalactic Database (NED) operated by the Jet Propulsion Laboratory, California Institute of Technology, under contract with the National Aeronautics and Space Administration. The research is partly based on data obtained from the Multimission Archive at the Space Telescope Science Institute (MAST). STScI is operated by the Association of Universities for Research in Astronomy, Inc., under NASA contract NAS5-26555. We are

grateful to Evgenii Churazov for his assistance in discussing the X-ray data and to Olga Sil'chenko, Victor Afanasiev and Natalia Sotnikova for useful comments; and also to our anonymous referee for his constructive advice that helped us to improve the paper. This work was supported by the Russian Foundation for Basic Research (project no. 09-02-00870). AM is also grateful to the 'Dynasty' Fund.

## REFERENCES

- Afanasiev V. L., Dodonov S. N., Moiseev A. V., 2001, in Ossipkov L. P., Nikiforov I. I., eds, *Stellar Dynamics: from Classic to Modern*, Saint Petersburg, p. 103
- Afanasiev V. L., Moiseev A. V., 2005, *Astronomy Letters*, 31, 193; astro-ph/0502095
- Allen M. G., Groves B. A., Dopita M. A., Sutherland R. S., Kewley L. J., 2008, *ApJS*, 178, 20
- Barnes J. E., Hernquist L. E., 1991, *ApJ*, 370, L65
- Barth A. J., Bentz M. C., Greene J. E., Ho L. C., 2008, *ApJ*, 683, L119
- Bekki K., Shioya Y., Whiting M., 2006, *MNRAS*, 371, 805
- Capetti A., Axon D. J., Macchetto F. D., Marconi A., Winge C., 1999, *ApJ*, 516, 187
- Chilingarian I., Prugniel Ph., Sil'chenko O., Koleva M., 2007, in Vazdekis A., Peletier R. F., eds., *Stellar Populations as Building Blocks of Galaxies*, *Proceedings of IAU Symposium*, 241, Cambridge University Press, p.17
- Ciroti S., Afanasiev V. L., Moiseev A. V., Botte V., Di Mille F., Dodonov S. N., Rafanelli P., Smirnova A. A., 2005, *MNRAS*, 360, 253
- Dahari O., 1985, *AJ*, 90, 1772
- De Robertis M. M., Yee H. K. C., Hayhoe K., 1998, *ApJ*, 496, 93
- Deo R. P., Crenshaw D. M., Kraemer S. B., 2006, *AJ*, 132, 321
- Erwin P., Beckman J. E., Pohlen M., 2005, *ApJ*, 626, L81
- Ferruit P., 2002, *RevMexAA (Serie de Conferencias)*, 13, 183
- García-Lorenzo B., Arribas S., Mediavilla, E., 2001, *A&A*, 787, 2001
- Gonzalez Delgado R. M., Perez E., Tadhunter C., Vilchez J. M., Rodriguez-Espinosa J. M., 1997, *ApJS*, 108, 155
- Heckman T. M., Armus L., Miley G. K., 1990, *ApJS*, 74, 833
- Hopkins P. F., Hernquist L., Cox T. J., Dutta S. N., Rothberg B., 2008, *ApJ*, 679, 156
- Hunt L. K., Malkan M. A., Salvati M., Mandolesi N., Palazzi E., Wade R., 1997, *ApJS*, 108, 229
- Keel W. C., 1996, *AJ*, 111, 696
- Kennicutt Jr. R. C., 1998a, *ARA&A*, 36, 189
- Kennicutt Jr. R. C., 1998b, *ApJ*, 498, 541
- Knapen J. H., 2005, *Ap&SS*, 295, 85
- Koleva M., Prugniel Ph., Bouchard A., Wu Y., 2009, *A&A*, in press, arXiv:0903.2979
- Komossa S., Xu D., Zhou H., Storchi-Bergmann T., Binette L., 2008, *ApJ*, 680, 926
- Levy V. V., 2000, *A&A Transactions*, 18, 621
- Li C., Kauffmann G., Heckman T. M., White S. D. M., Jing Y. P., 2008, *MNRAS*, 385, 1915
- Lumsden S. L., Heisler C. A., Bailey J. A., Hough J. H., Young S., 2001, *MNRAS*, 327, 459
- Maiolino R., Ruiz M., Rieke G. H., Papadopoulos P., 1997, *ApJ*, 485, 552
- Martini P., 2004, in Storchi-Bergmann T., Ho L. C., Schmitt H. R., eds, *The Interplay Among Black Holes, Stars and ISM in Galactic Nuclei Vol. 222 of IAU Symposium*, p. 235
- Martini P., Pogge R. W., 1999, *AJ*, 118, 2646
- Martini P., Pogge R. W., Ravindranath S., An J. H., 2001, *ApJ*, 562, 139
- Moiseev A. V., 2001, *Bull. Spec. Astrophys. Obs.*, 51, 11; astro-ph/0111219
- Moiseev A. V. 2002, *Bull. Spec. Astrophys. Obs.*, 54, 74; astro-ph/0211104
- Moiseev A. V., Egorov O. V., 2008, *Astrophys Bull.*, 63, 193; arXiv: 0805.2367 [astro-ph]
- Moiseev A. V., Valdés J. R., Chavushyan V. H., 2004, *A&A*, 421, 433
- Muñoz Marín V. M., González Delgado R. M., Schmitt H. R., Cid Fernando R., Pérez E., Storchi-Bergmann T. et al., 2007, *AJ*, 134, 648
- Osterbrock D. E., 1989, *Astrophysics of Gaseous Nebulae and Active Galactic Nuclei*. University Science Books, Mill Valley, CA
- Pérez García A. M., Rodríguez Espinosa J. M., 2001, *ApJ*, 557, 39
- Rothberg B., Joseph R. D., 2004, *AJ*, 128, 2098
- Sánchez-Blázquez P., Peletier R. F., Jiménez-Vicente J., Cardiel N., Cenarro A. J. et al., 2006, *MNRAS*, 371, 703
- Schmitt H. R., 2001, *AJ*, 122, 2243
- Schweizer F., Seitzer P., 1988, *ApJ*, 328, 88
- Sil'chenko O. K., Moiseev A. V., 2006, *AJ*, 131, 1336
- Sil'chenko O. K., Vlasyuk V. V., Alvarado F., 2001, *AJ*, 121, 2499
- Shalyapina L.V., Moiseev A. V., Yakovleva V. A., Hagen-Thorn V. A., Burenkov A. N., 2004, *Astronomy Letters*, 30, 1
- Smirnova A. A., Moiseev A. V., Afanasiev V. L., 2006, *Astronomy Letters*, 32, 520; astro-ph/0607163
- Smirnova A. A., Gavrilović N., Moiseev A. V., Popović L. Č., Afanasiev V. L., Jovanović P., Dačić M., 2007, *MNRAS*, 377, 480
- Spoon H. W. W., Keane J. V., Tielens A. G. G. M., Lutz D., Moorwood A. F. M., Laurent O., 2002, *A&A*, 385, 1022
- Springel V., Di Matteo T., Hernquist L., 2005, *ApJ*, 620, L79
- Ulvestad J. S., 1986, *ApJ*, 310, 136
- Veilleux S., Cecil G., Bland-Hawthorn J., 2005, *ARA&A*, 43, 769
- Veilleux S., Osterbrock D. E., 1987, *ApJS*, 63, 295
- Vorontsov-Vel'yaminov B. A., 1977, *A&AS*, 28, 1
- Wehner E. H., Gallagher J. S., 2005, *ApJ*, 618, L21
- Zimmermann H.-U., Boller T., Döbereiner S., Pietsch W., 2001, *A&A*, 378, 30